Biochimica et Biophysica Acta 1858 (2016) 1443–1450

Contents lists available at ScienceDirect

Biochimica et Biophysica Acta

journal homepage: www.elsevier.com/locate/bbamem

Relating structure and internalization for ROMP-based protein mimics

Coralie M. Backlund [a], Toshihide Takeuchi [b], Shiroh Futaki [c], Gregory N. Tew [d,*]

[a] Department of Polymer Science & Engineering, University of Massachusetts, Amherst, MA 01003, USA
[b] Department of Veterinary & Animal Sciences, University of Massachusetts, Amherst, MA 01003, USA
[c] Molecular and Cellular Biology Program, University of Massachusetts, Amherst, MA 01003, USA
[d] Institute for Chemical Research, Kyoto University, Uji, Kyoto 611-0011, Japan

ARTICLE INFO

Article history:
Received 25 November 2015
Received in revised form 24 February 2016
Accepted 29 March 2016
Available online 31 March 2016

Keywords:
Protein transduction domains
TAT
Internalization
Cell-penetrating peptide

ABSTRACT

Elucidating the predominant cellular entry mechanism for protein transduction domains (PTDs) and their synthetic mimics (PTDMs) is a complicated problem that continues to be a significant source of debate in the literature. The PTDMs reported here provide a well-controlled platform to vary molecular composition for structure activity relationship studies to further our understanding of PTDs, their non-covalent association with cargo, and their cellular internalization pathways. Specifically, several guanidine rich homopolymers, along with an amphiphilic block copolymer were used to investigate the relationship between structure and internalization activity in HeLa cells, both alone and non-covalently complexed with EGFP by flow cytometery and confocal imaging. The findings indicate that while changing the amount of positive charge on our PTDMs does not seem to affect the endosomal uptake, the presence of hydrophobicity appears to be a critical factor for the polymers to enter cells either alone, or with associated cargo.

1. Introduction

Over the past decade, intracellular targeting has become an emerging area of research in drug delivery, diagnostics, and chemical biology. However, cell membranes are impermeable to most macromolecules and small molecules. One exception seems to be a class of cell-penetrating peptides (CPPs) known as protein transduction domains (PTDs) and their synthetic mimics (PTDMs). Intracellular delivery using PTDs remains a promising method for introducing exogenous macromolecules into cells [1,2].

The Tat (transactivator of transcription) protein of the human immunodeficiency virus type 1 (HIV-1), discovered in 1988, was the first identified PTD [3]. Later, it was determined that an eleven amino acid residue sequence (YGRKKRRQRRR), rich in basic amino acids, was required for translocation of Tat through the plasma membrane [4,5]. In the last two decades, over 100 CPP sequences have been published and this number continues to expand as more is learned about these molecules [6]. These CPPs are usually small, cationic peptides, some of which contain a hydrophobic component. Their main feature is their ability to cross cell membranes either on their own or conjugated to a range of biomolecules, such as peptides, proteins, liposomes, and nanoparticles. This is possible at micro-molar concentrations without causing significant membrane damage [7]. Synthetic CPPs deviate from naturally occurring protein sequences and are either designed to mimic their structures and compositions or to produce amphipathic α-helical structures. Examples are the model amphipathic peptide (MAP) and oligoarginine sequences, such as **R8**. These synthetic CPPs have also been covalently attached to various macromolecules and their internalization has been studied [8,9].

Intracellular delivery of large molecules, including macromolecules and liposomes, often involves the uptake of PTD(M) complexes by endocytosis [10]. Arginine-rich PTDMs have been proposed to induce macropinocytosis, which in turn leads to accelerated internalization of cell surface adsorbed PTDMs and PTDM-cargo complexes [11–13]. Since macropinocytosis is considered a non-specific fluid phase endocytosis pathway, its induction should facilitate indiscriminate uptake [14]. The endosomal route usually finishes with the acidic and proteolytic degradation of the lysosomal content, thus preventing the delivered cargo from reaching its cytosolic targets [15]. The release of biologically active cargo from endosomes is a necessary step and is a major limitation for this type of uptake. [7].

A second mode of uptake is direct translocation, an energy-independent penetration pathway in which a transient destabilization occurs in the membrane, followed by the rapid intracellular localization of the peptide [16–18]. For drug delivery purposes, it is preferred that molecules enter cells by direct translocation, as this pathway does not incur endosomal entrapment. Changes in hydrophobicity have been implicated as the driving factor for arginine-rich molecules to cross cell membranes through direct translocation [19]. Additionally, cell surface concentrations of arginine-rich PTDMs may also play a role in peptide entry into cells [20]. Some peptides exceeding a threshold concentration have been observed to directly penetrate the membrane, while at lower concentrations uptake is primarily by endocytosis [18,21,22].

* Corresponding author at: 120 Governors Dr Amherst, MA 01003

http://dx.doi.org/10.1016/j.bbamem.2016.03.024
0005-2736/

A change in membrane curvature is required for both endocytosis and direct penetration, which can be facilitated by CPP–membrane interactions [23]. Decoupling endocytosis from direct penetration remains largely unsolved. The use of endocytosis inhibitors may alter other cellular processes, making deconvolution of the treatments difficult [24]. Cooling cells to 4 °C provides another challenge in that cooler temperatures affect the membrane fluidity making it more rigid and therefore more permeable to larger molecules [25].

While many CPPs and their mimics show high membrane permeability and efficient cargo delivery, the mechanisms by which PTDMs and PTDM-cargo complexes traverse cell membranes are not completely understood and are highly debated in the literature [24]. The methods by which arginine-rich PTDs are internalized depend on the physiochemical properties of the PTDs, the cargo molecules, and cell type, as well as a variety of other parameters [24]. Therefore, it is not surprising that the predominant internalization mechanism may deviate depending on the attached cargo [24]. Understanding this cellular uptake mechanism of CPPs under physiological conditions is important for the development of appropriate strategies for therapeutic applications both *in vitro* and *in vivo*. Since several routes may exist simultaneously, it is important to correlate the uptake pathway with the biological response associated with a specific cargo *e.g.* if the target of the cargo is cytosolic or endosomal. These parameters will enable the design of materials to target specific routes of internalization.

Creating polymeric scaffolds with CPP-like internalization and cargo delivery properties have recently emerged as a new research direction. [26,27] Polymers allow for the use of different, easily tailored chemistries and architectures for investigating structure activity relationships, while tuning for efficient cargo delivery. Using ring-opening metathesis polymerization (ROMP), which is functional group tolerant, well-controlled, and versatile, a highly efficient set of synthetic PTDMs has been developed [26,28–35]. These designs, based on polyarginine, are guanidinium-rich and allow for non-covalent internalization of various biological cargos [31–33]. The ability to easily include diverse functional groups allows us to probe architecture, molecular composition, and molecular weight in a controlled manner, mimicking peptide synthesis [29,32].

Polymeric mimics offer a controlled way to explore the effects of structure and macromolecular composition on internalization efficiency. Using **R8** as inspiration and a benchmark, a [28,31–36] set of four homopolymers and one block copolymer (Fig. 1) were chosen to investigate the impact of polymer structure and backbone on internalization efficiency in HeLa cells.

Determining the parameters that dictate the predominant method of internalization is crucial to the understanding and optimization of CPPs and their mimics. In this work, we use the delivery of cargo by synthetic PTDMs as a handle for elucidating the intracellular pathways through which these molecules enter. More specifically, HeLa cells were treated with the chosen PTDMs, either with a FITC label or associated with fluorescent protein, allowing for confocal laser scanning microscopy (CLSM) and flow cytometry (FCM) analysis. Imaging explicates the predominant mode of uptake as endosomal uptake and allows us to address some of the more difficult questions regarding polymer-cell interactions, while flow cytometry generates quantitative results (on a much larger number of cells) that can be used to verify trends seen with imaging. From these results, we determined that concentration and polymer architecture have little effect on the mode of translocation into the cell, but rather play a more important role in how much cargo they are able to deliver.

2. Materials and methods

2.1. PTDM synthesis

Monomers and PTDMs were synthesized according to established literature procedures [28,31,34]. In brief, the monomers were synthesized by ring-opening a Diels–Alder anhydride adduct with a desired

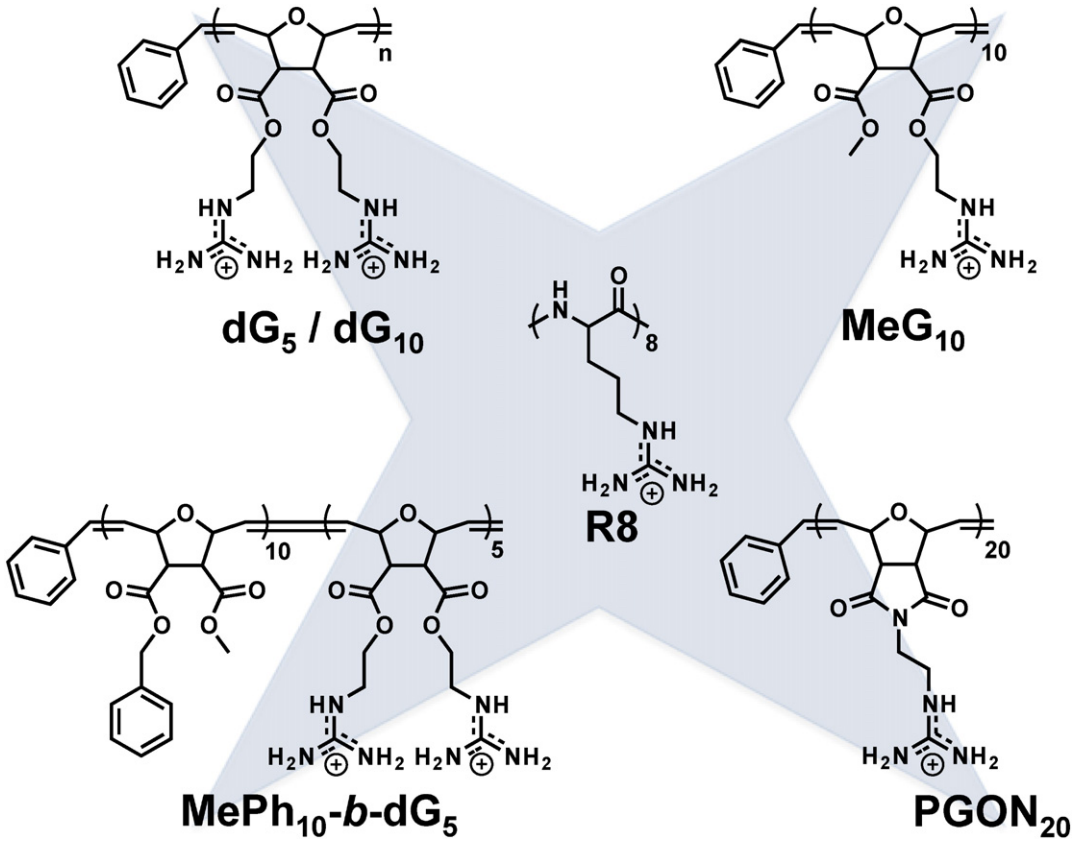

Fig. 1. Polymers of interest: **R8** inspired the design of $\mathbf{dG_5}$ (n = 5), $\mathbf{dG_{10}}$ (n = 10), $\mathbf{MeG_{10}}$, $\mathbf{PGON_{20}}$, and $\mathbf{MePh_{10}}$-***b***-$\mathbf{dG_5}$.

alcohol, using 4-dimethylaminopyridine (DMAP) as a catalyst, to obtain a mono-functional intermediate. This was followed by 1-ethyl-3-(3-dimethylaminopropyl)carbodiimide (EDC) coupling with another equivalent of alcohol to introduce the second functionality. The desired PTDMs were subsequently synthesized by ROMP using the Grubbs' third generation catalyst in dichloromethane (CH_2Cl_2), with dispersity indices under 1.1 ($Đ = M_w/M_n$). Polymerizations were terminated using ethyl vinyl ether, and polymers were deprotected using a 1:1 ratio of trifluoroacetic acid (TFA): CH_2Cl_2. The final products were purified by dialysis against RO water, recovered by lyophilization, and stored at −20 °C.

A second set of PTDMs was terminated with a previously reported activated ester for functionalization with Alexa Fluor 488 dye [37]. The PTDMs were allowed to stir in an excess of dye for 3 days. Unreacted dye was removed using a silica column. They were then deprotected with a 1:1 ratio of TFA:CH_2Cl_2, dialyzed against RO water, and lyophilized. All polymers were dissolved in sterile DMSO to make 1 mM stock solutions and were stored at −20 °C until their use.

2.2. Internalization of FITC-labeled PTDMs

HeLa cells were seeded at 1×10^4 cells/2 mL of α-MEM with 10% FBS on 35 mm glass bottom plates 48 h prior to treatment and cultured at 37 °C and 5% CO_2. FITC-PTDMs were diluted 1:10 in PBS and then to a final concentration of 5, 10, and 20 μM in α-MEM with 10% FBS. Cells were washed with warm, fresh, complete media and 200 μL of PTDM solution was applied on top of the glass bottom. Cells were incubated for 1 h and then washed three times with cold media to remove excess PTDM and to slow cellular function. Cells were covered in 1 mL of cold media and imaged at 60× with confocal laser scanning microscope (CLSM).

To investigate colocalization with lysosomes, cells were treated with 5 μM FITC-PTDM and 20 nM lysotracker red for 1 h. Samples were analyzed in a similar manner to the internalization experiments using both red and green lasers on the CLSM. Correlation between the location of the lysotracker and the FITC-PTDM was determined by Pearson's colocalization coefficient (PCC) using Autoquant software.

2.3. EGFP delivery

EGFP was prepared using previously reported methods [18]. HeLa cells were seeded at 1×10^6 cells/2 mL of α-MEM with 10% FBS on 35 mm glass bottom plates and 1×10^5 cells/1 mL on 12-well plates 48 h prior to treatment and cultured at 37 °C and 5% CO_2. Polymer was complexed with 2 μg of EGFP using previously reported methods at a ratio of 20:1 PTDM to protein (unpublished). Cells were treated for 4 h with the polymer/protein complexes in a total volume of 1 mL α-MEM with 10% FBS. Before imaging, cells were washed three times with cold media and covered in 1 mL fresh, cold α-MEM with 10% FBS. Cells were imaged using CLSM at 60×. To prepare for flow cytometry (FCM), the cells were trypsinized and washed three times with a 20 U/mL heparin solution before being suspended in PBS with 0.2 wt% FBS.

To determine if the 30 min incubation period was required for optimal uptake, cells were treated with PTDMs not incubated with protein at the same concentration. PTDMs and protein were diluted as stated above and added drop-wise without mixing into the media. Uptake was analyzed by FCM to determine the percentage of cells that internalized the polymer, as well as the median fluorescence intensity (MFI) of the cells.

3. Results and discussion

3.1. Polymer design and synthesis

In this study, PTDMs were designed to resemble **R8** (Fig. 1), with $\mathbf{MeG_{10}}$ containing one guanidinium group per repeat unit, yielding about 10 positive charges per polymer. The diguanidine (**dG**) series ($\mathbf{dG_5}$ and $\mathbf{dG_{10}}$) were designed to create a higher density of guanidinium groups to better mimic the distribution of charge along the peptide backbone. $\mathbf{dG_5}$, with about 10 positive charges, correlates to **R8** in that it has approximately the same number of guanidinium groups, but only half the number of repeat units, while $\mathbf{dG_{10}}$ has approximately the same number of repeat units as **R8**, but has twice as many guanidinium moieties, or about 20 positive charges. A second ROMP backbone, the imide-based poly-guanidinium oxanorbornene (**PGON**), was added to the series because of its high membrane activity with lipid vesicles [34]. Since $\mathbf{PGON_{20}}$ only contains one guanidinium group per repeat unit, a length of 20 was chosen for comparison to $\mathbf{dG_{10}}$, resulting in about 20 positive charges along the length of the polymer. Lastly, a block copolymer with 10 hydrophobic and 5 diguanidinium monomers ($\mathbf{MePh_{10}}$-***b***-$\mathbf{dG_5}$) was included because of its efficient non-covalent protein delivery into Jurkat T Cells (unpublished), predominantly due to the added hydrophobicity that has been shown to be required for efficient protein delivery. Added hydrophobicity, which has been predicted to increase saddle splay curvature, combined with lipid head-group coordination by guanidinium groups, promotes membrane permeation [23]. These polymers were all synthesized with and without covalently attached FITC labels.

3.2. Internalization of FITC-labeled PTDMs

HeLa cells were treated with FITC-PTDMs for 1 h and imaged using a CLSM, as shown in Fig. 2A, and also analyzed using FCM (Fig. 2B and C). Images revealed that $\mathbf{dG_5}$ and $\mathbf{MeG_{10}}$ exhibited low cell entry. $\mathbf{MeG_{10}}$ appeared to aggregate extensively and was dropped from further studies. This aggregation could be due to the overall charge density being too low, with one charge per monomer, allowing the PTDMs to have a greater self-affinity than for the solution or cell membranes. Both homopolymers with 20 guanidinium units ($\mathbf{PGON_{20}}$ and $\mathbf{dG_{10}}$) demonstrated efficient internalization, particularly $\mathbf{PGON_{20}}$. This is unsurprising, as previous reports have shown that it is highly membrane active in biophysical assays compared to other homopolymers produced in this group. [28] The block copolymer PTDM also showed punctate internalization throughout the cell with high efficiency for all imaged cells.

The median fluorescence intensities (MFIs), shown in Fig. 2B, corroborate the confocal images. An artificially high MFI is expected from $\mathbf{MeG_{10}}$, since large aggregates were seen in and on cells in the confocal images. $\mathbf{dG_{10}}$ and $\mathbf{PGON_{20}}$ showed high membrane activity (see Fig. 2) and consequently resulted in a 3 to 4 fold higher MFI than $\mathbf{MePh_{10}}$-***b***-$\mathbf{dG_5}$. We speculate that efficient internalization with the dye requires a combination of a critical hydrophobic component and charge content that is not met with $\mathbf{dG_5}$. Along this line of thought, the internalization of $\mathbf{PGON_{20}}$ could be attributed to its increased length. Although $\mathbf{MePh_{10}}$-***b***-$\mathbf{dG_5}$ resulted in a low MFI, the punctate fluorescence was prevalent in all imaged cells, and more than 95% of the cell population was fluorescent.

While punctate fluorescence is easily visible, the location and type of endosomal compartments were still in question. To determine if the PTDMs were trapped in endosomes and if those endosomes were bound for degradation, colocalization with lysotracker was investigated.

3.3. Colocalization with lysosomes

To compare the location of internalized PTDMs with late endosomal compartments, cells were treated with lysotracker red during the treatment with FITC-PTDMs (Fig. 3). FITC-PTDMs (green) trapped in late endosomes should colocalize with the lysotracker red, indicated by yellow.

While the diester homopolymers ($\mathbf{dG_5}$ and $\mathbf{dG_{10}}$) proved less successful at internalization, **R8**, $\mathbf{PGON_{20}}$, and $\mathbf{MePh_{10}}$-***b***-$\mathbf{dG_5}$ showed robust internalization in punctate structures. Some of the $\mathbf{MePh_{10}}$-***b***-$\mathbf{dG_5}$

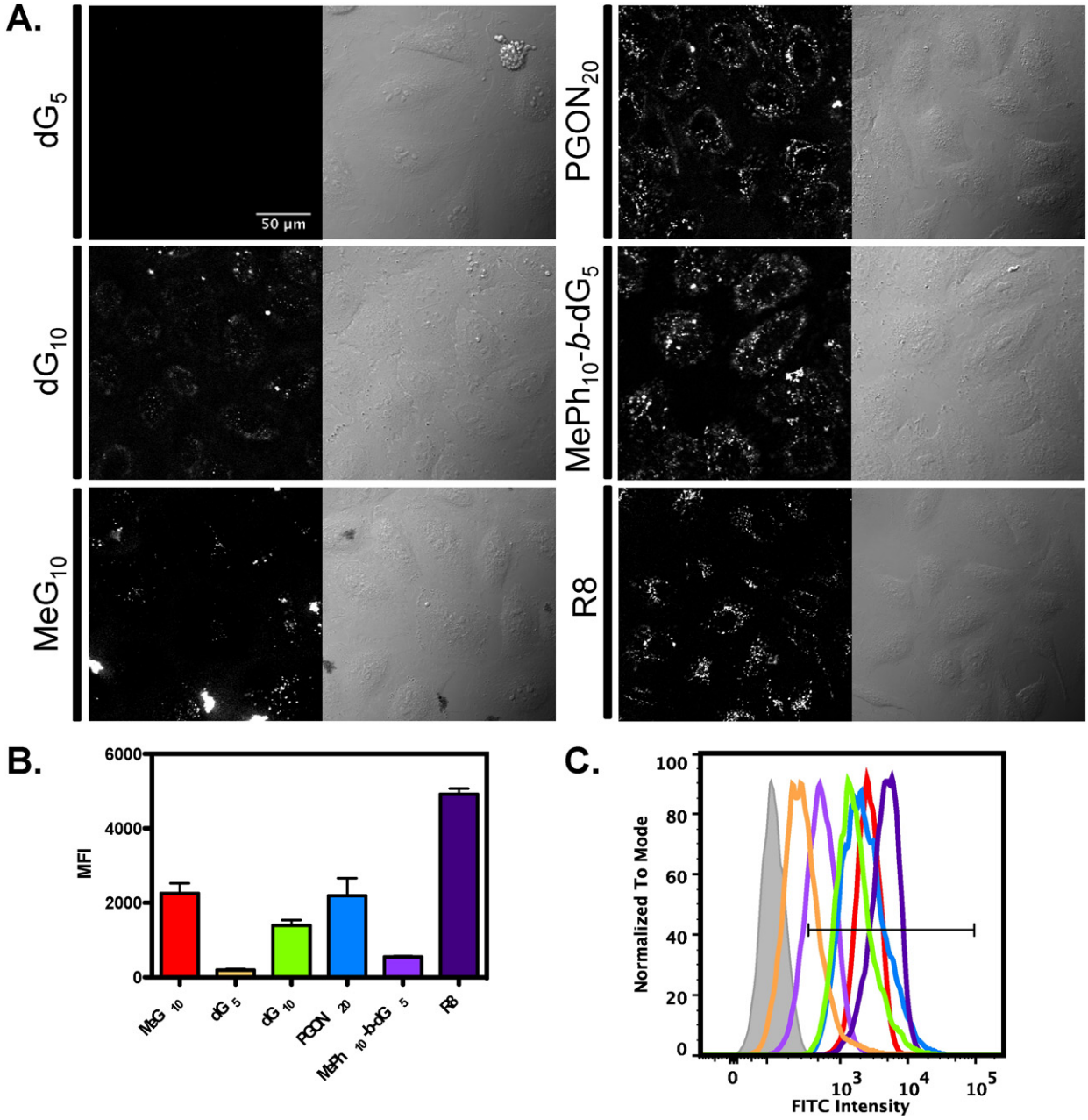

Fig. 2. Internalization of FITC-labeled PTDMs into HeLa cells. Cells were treated with 5 μM PTDM for 1 h and imaged with a CLSM (A) and assessed for fluorescence internalization using a flow cytometer for both MFI (B) and a positive shift in intensity from the blank (gray) in FCM histograms (C). Polymer colors in (B) correspond to their respective shifts in (C).

appears to overlap with the lysotracker red, suggesting that endosomal entrapment is involved in internalization. The enlargement of **MePh$_{10}$-*b*-dG$_5$** with lysotracker red is overlapped (yellow), but mutual exclusion of the polymer (green) from the late endosomes (red) also exists. The Pearson's Correlation Coefficient (PCC) for the homopolymer PTDMs and **R8** was approximately 0.3 for all samples, suggesting little to no correlation between the lysotracker and the polymer, while **MePh$_{10}$-*b*-dG$_5$** had a PCC of 0.8, suggesting high colocalization with the late endosomes. In other words, the hydrophobic PTDM was able to internalize in late endosomes, but was not exclusively located there. This suggests that while some PTDM is permanently trapped in endosomes, it is not necessarily all destined for degradation. Additionally, escape from endosomal compartments cannot be dismissed. Longer time periods of this study with a more photo stable dye would allow for further investigation on the kinetics of our polymers within cells, but was not the focus of this study.

3.4. Concentration dependence

Since the mechanism of uptake can be dependent on the experimental conditions, an increase in concentration of **MePh$_{10}$-*b*-dG$_5$** and **R8** was used to investigate the effect of concentration on the predominant mode of internalization. Increasing the concentration appeared to increase the amount of **R8** and **MePh$_{10}$-*b*-dG$_5$** that entered the cell, although with increasing cytotoxicity (Fig. 4A and SI Figs. 2–7). Confocal images showed that at higher concentrations of both PTDMs, cells began to bleb and appeared unhealthy. More aggregated punctate fluorescence suggests compromise of the cellular membrane. The increase in fluorescence intensity and decrease in viability (using 7-AAD) with increasing concentration were quantified using flow cytometry. As shown in Fig. 4, **R8** decreases to approximately 20% viability, while **MePh$_{10}$-*b*-dG$_5$** showed lower induced apoptosis even at higher concentrations of PTDMs despite considerable blebbing apparent in the CLSM

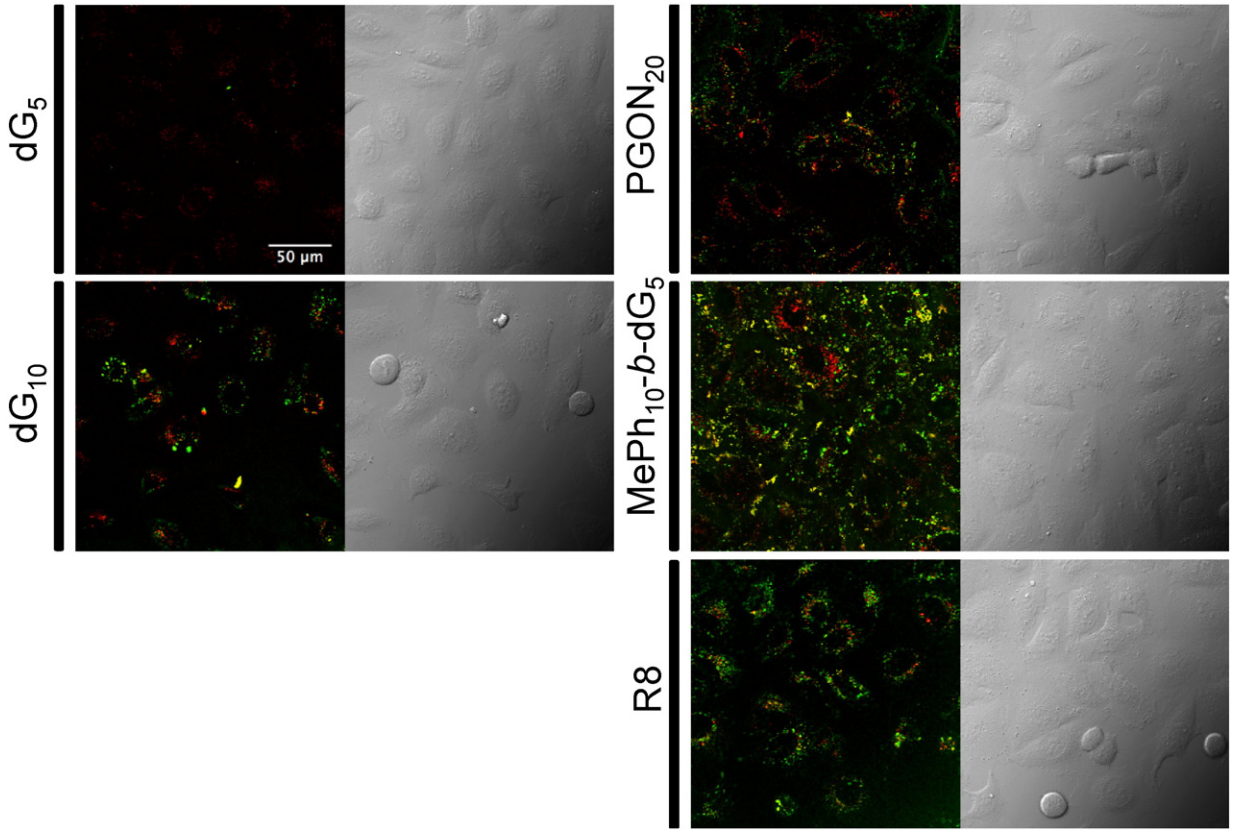

Fig. 3. Internalization of FITC-PTDMs (green) in the presence of lysotracker (red) in HeLa cells. Cells were treated with 5 μM FITC-labeled polymer and lysotracker red for 1 h and imaged using a CLSM.

images. There was no change in mechanism observed, as fluorescence remained punctate in all images, even after 4 h. Although persistent punctate structures would suggest the inability of the PTDMs to escape endosomes over short periods of time, it is difficult to exclude some PTDM endosomal escape since these fewer dispersed molecules would appear much dimmer by CLSM analysis.

3.5. EGFP delivery

Polymers were tested for transduction efficiency with enhanced green fluorescent protein (EGFP) as an indication of internal cell location and delivery efficiency. The PTDMs and protein were incubated for 30 min to allow for the formation of non-covalent complexes and then applied drop-wise to HeLa cells. At 4 hours, all homopolymer PTDMs and **R8** proved to be ineffective at delivering protein into the cell, showing limited uptake in both the microscope images and FCM data (Fig. 5). The block copolymer showed significantly higher internalization, but was still punctate, suggesting entrapment in endosomes within the observed time periods. None of the PTDMs or **R8** showed any cytotoxic effects compared to the untreated sample, as determined by 7AAD during flow analysis, see SI Fig. 8 for graphical representation. While the lack of delivery with the diester homopolymer PTDMs was unsurprising because of their poor internalization with the dye, it is interesting that **PGON$_{20}$** was unable to facilitate protein internalization. This could be attributed to its lack of a defined hydrophobic segment. **MePh$_{10}$-*b*-dG$_5$** was expected to have high delivery, as **R8** has been shown to be more effective with a hydrophobic component attached [38]. As demonstrated here and by others, the hydrophobic domain of the PTDM is important to protein internalization [38,39]. The block copolymer outperformed all other polymers tested at protein delivery yielding an MFI around 20 times higher, as determined by FCM (Fig. 5B). This was corroborated with confocal images, which revealed both punctate and diffuse fluorescence within the imaged cells (Fig. 5A).

Additionally, complex formation was tested to determine if the PTDMs merely compromise the cell membrane allowing protein into the cytosol, or if they actively facilitate transport across the membrane. Cells were treated with **MePh$_{10}$-*b*-dG$_5$** and **R8** complexed with protein for 30 min at room temperature and were compared with cells treated directly with the PTDMs followed by protein, which were given no time to form a complex. The flow cytometry data, highlighted in Fig. 5C, showed internalization for the cells treated with **MePh$_{10}$-*b*-dG$_5$** and protein complex, but not for those treated with the PTDMs and protein independently. This suggests that **MePh$_{10}$-*b*-dG$_5$** does not merely interact with the membrane to allow indiscriminant uptake of proteins in the cytosol, but rather an incubation time is required for the PTDMs to form complexes with the proteins.

4. Conclusion

While determining the predominant mode of internalization for CPPs remains a challenge, using PTDMs to advance the understanding of how structure influences uptake activity is critical to improving design parameters for efficient internalization. By examining changes in molecular composition in relation to their ability to enter cells when complexed with cargo, PTDMs can be enhanced to deliver specific molecules into the cell. Here, we performed common methods to assess internalization mechanisms and efficiency for guanidinium-containing PTDMs both alone and non-covalently complexed to cargo. This provides the first side-by-side studies for this class of PTDMs and **R8** with respect to cellular internalization. Homopolymer PTDMs proved to be inefficient at entering cells, with the exception of **PGON$_{20}$**, which was even able to enter cells at a higher capacity than the block copolymer PTDM **MePh$_{10}$-*b*-**

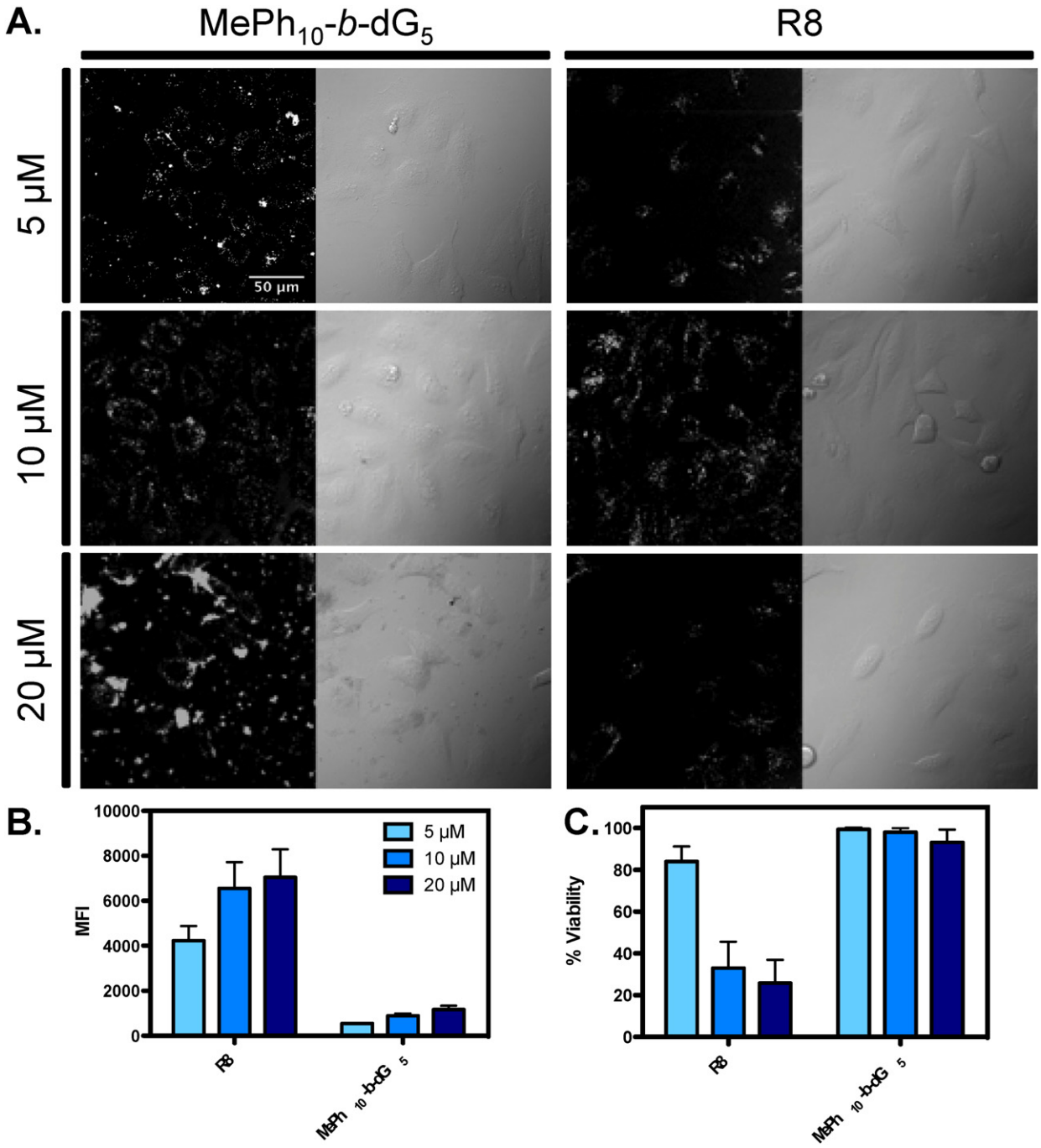

Fig. 4. Effects of concentration on FITC-labeled polymer internalization. Concentration dependence for **$MePh_{10}$-*b*-dG_5** and **R8** labeled with FITC at 5, 10, and 20 μM (A). HeLa cells were treated with 1 h with PTDMs and imaged with a CLSM and assessed for MFI (B) and viability (C) using flow cytometry.

dG_5. Increasing the concentration of the PTDMs led to improved internalization but also to higher cytotoxicity, a common observation across PTDMs. None of the homopolymer PTDMs were able to facilitate the delivery of EGFP, while **$MePh_{10}$-*b*-dG_5** proved to be exceptionally efficient. Additionally, **$MePh_{10}$-*b*-dG_5** was the only polymer that also localized with late endosomes, suggesting endosomal entrapment for some of the complexes on the time scale used in this study. This finding highlights the importance of hydrophobic segments for efficient cargo delivery by PTDMs and that these structural changes influence the balance of pathways. These polymers remained punctate in the case of internalization for FITC-labeling and protein delivery, suggesting that endosomal uptake is the predominant mode of internalization. Findings will contribute to future design considerations for intracellular delivery systems and aid in our understanding of the modes of internalization for arginine-rich molecular transporters.

Transparency document

The Transparency document associated with this article can be found, in online version.

Acknowledgments

The authors acknowledge the NSF (DMR-1308123) Eastern Asian and Pacific Summer Internship (EAPSI) (IIA-1414767)

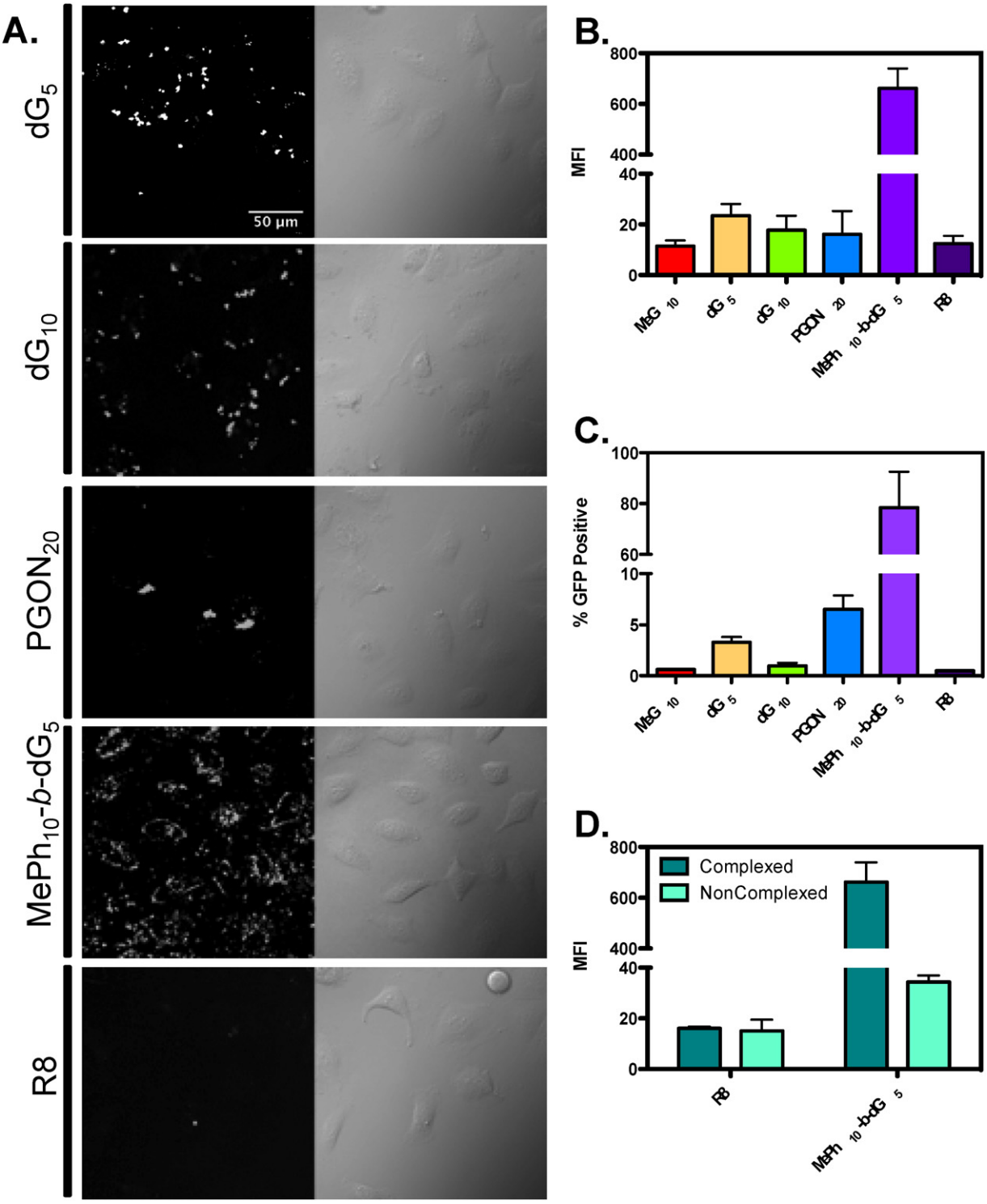

Fig. 5. EGFP delivery into HeLa cells with unlabeled PTDMs. EGFP was complexed with PTDMs for 30 min at a molar ratio of 20:1. HeLa cells were treated with the complexes for 4 hours to observe internalization. Cells were imaged using a CLSM (A). Internalization efficiency as determined by MFI (B) and percent uptake (C) was confirmed using FCM to quantitate the delivery of EGFP. Complexed **$MePh_{10}$-*b*-dG_5** with protein was tested in relation to non-complexed polymer and protein compared to **R8** with and without the protein (D).

fellowship program and the Japanese Society for the Promotion of Science (JSPS) for funding on this project. NSF Authors would like to thank Brittany deRonde for help with editing the manuscript and Katie Gibney for help with polymer synthesis. A special thanks is extended to Joel Sarapas for manuscript help, synthesis advice, and donation of the activated ester. Additional thanks goes to Tomo Murayama, Misao Akishiba, Akihiko Oku, and Yashimasa Kawaguchi for the help in setting up experiments and consulting on techniques.

Appendix A. Supplementary data

Supplementary data to this article can be found online at http://dx.doi.org/10.1016/j.bbamem.2016.03.024.

References

[1] M.C. Morris, S. Deshayes, F. Heitz, G. Divita, Biol. Cell. 100 (2008) 201–217.
[2] M. Pooga, Ü. Langel, Methods Mol. Biol. 1324 (2015) 3–28.
[3] A.D. Frankel, C.O. Pabo, Cell 55 (1988) 1189–1193.
[4] M. Green, P.M. Loewenstein, Cell 55 (1988) 1179–1188.
[5] E. Vivès, P. Brodin, B.J. Lebleu, Biol. Chem. 272 (1997) 16010–16017.
[6] M. Lindgren, U. Langel, Methods Mol. Biol. 683 (2011) 3–19.
[7] I. Martín, M. Teixidó, E. Giralt, Curr. Pharm. Des. 19 (2013) 2924–2942.
[8] J. Oehlke, A. Scheller, B. Wiesner, E. Krause, M. Beyermann, E. Klauschenz, M. Melzig, M. Bienert, Biochim. Biophys. Acta 1414 (1998) 127–139.
[9] S. Futaki, T. Suzuki, W. Ohashi, T. Yagami, S. Tanaka, K. Ueda, Y.J. Sugiura, Biol. Chem. 276 (2001) 5836–5840.
[10] I. Nakase, G. Tanaka, S. Futaki, Mol. BioSyst. 9 (2013) 855–861.
[11] S.D. Conner, S.L. Schmid, Nature 422 (2003) 37–44.
[12] J.S. Wadia, R.V. Stan, S.F. Dowdy, Nat. Med. 10 (2004) 310–315.
[13] I. Nakase, M. Niwa, T. Takeuchi, K. Sonomura, N. Kawabata, Y. Koike, M. Takehashi, S. Tanaka, K. Ueda, J.C. Simpson, A.T. Jones, Y. Sugiura, S. Futaki, Mol. Ther. 10 (2004) 1011–1022.
[14] A.T. Jones, J. Cell Mol. Med. 11 (2007) 670–684.
[15] A. El-Sayed, S. Futaki, H. Harashima, AAPS J. 11 (2009) 13–22.
[16] P.E. Thorén, D. Persson, P. Isakson, M. Goksör, A. Onfelt, B. Nordén, Biochem. Biophys. Res. Commun. 307 (2003) 100–107.
[17] J.B. Rothbard, T.C. Jessop, R.S. Lewis, B.A. Murray, P.A. Wender, J. Am. Chem. Soc. 126 (2004) 9506–9507.
[18] M. Kosuge, T. Takeuchi, I. Nakase, A.T. Jones, S. Futaki, Bioconjug. Chem. 19 (2008) 656–664.
[19] H.D. Herce, A.E. Garcia, M.C. Cardoso, J.Am. Chem. Soc. 136 (2014) 17459–17467.
[20] H.D. Herce, A.E. Garcia, J. Litt, R.S. Kane, P. Martin, N. Enrique, A. Rebolledo, V. Milesi, Biophys. J. 97 (2009) 1917–1925.
[21] M.M. Fretz, N.A. Penning, S. Al-Taei, S. Futaki, T. Takeuchi, I. Nakase, G. Storm, A.T. Jones, Biochem. J. 403 (2007) 335–342.
[22] R. Brock, Bioconjug. Chem. 25 (2014) 863–868.
[23] N.W. Schmidt, M. Lis, K. Zhao, G.H. Lai, A.N. Alexandrova, G.N. Tew, G.C. Wong, J.Am. Chem. Soc. 134 (2012) 19207–19216.
[24] F. Madani, S. Lindberg, U. Langel, S. Futaki, A. Gräslund, J. Biophys. 2011 (2011) 414729.
[25] J. Pae, P. Säälik, L. Liivamägi, D. Lubenets, P. Arukuusk, Ü. Langel, M. Pooga, J. Control. Release 192 (2014) 103–113.
[26] B.M. deRonde, G.N. Tew, Biopolymers 104 (2015) 265–280.
[27] E.G. Stanzl, B.M. Trantow, J.R. Vargas, P.A. Wender, Acc. Chem. Res. 46 (2013) 2944–2954.
[28] A. Som, A.O. Tezgel, G.J. Gabriel, G.N. Tew, Angew. Chem. Int. Ed. Eng. 50 (2011) 6147–6150.
[29] F. Sgolastra, B.M. deRonde, J.M. Sarapas, A. Som, G.N. Tew, Acc. Chem. Res. 46 (2013) 2977–2987.
[30] A. Som, A. Reuter, G.N. Tew, Angew. Chem. Int. Ed. Eng. 51 (2012) 980–983.
[31] A.Ö. Tezgel, J.C. Telfer, G.N. Tew, Biomacromolecules 12 (2011) 3078–3083.
[32] F. Sgolastra, L.M. Minter, B.A. Osborne, G.N. Tew, Biomacromolecules 15 (2014) 812–820.
[33] A.Ö. Tezgel, G. Gonzalez-Perez, J.C. Telfer, B.A. Osborne, L.M. Minter, G.N. Tew, Mol. Ther. 21 (2013) 201–209.
[34] A. Hennig, G.J. Gabriel, G.N. Tew, S. Matile, J.Am. Chem. Soc. 130 (2008) 10338–10344.
[35] G.J. Gabriel, A.E. Madkour, J.M. Dabkowski, C.F. Nelson, K. Nüsslein, G.N. Tew, Biomacromolecules 9 (2008) 2980–2983.
[36] B.M. deRonde, A. Birke, G.N. Tew, Chemistry 21 (2015) 3013–3019.
[37] A.E. Madkour, A.H. Koch, K. Lienkamp, G.N. Tew, Macromolecules 43 (2010) 4557–4561.
[38] K. Takayama, H. Hirose, G. Tanaka, S. Pujals, S. Katayama, I. Nakase, S. Futaki, Mol. Pharm. 9 (2012) 1222–1230.
[39] K. Takayama, I. Nakase, H. Michiue, T. Takeuchi, K. Tomizawa, H. Matsui, S. Futaki, J. Control. Release 138 (2009) 128–133.